Paper

Application of Fast Biorthogonal Spline Wavelet Transform in Automatic Inspection

Huiqin Jiang* Non-member
Jianming Lu* Member
Takashi Yahagi* Non-member

In the development of an automatic inspection device for inspecting the quality of printed circuit boards, it is necessary to be able to detect precisely and quickly the position of the demarcation line between two very close components on a printed circuit board. In this study, first this problem is changed to the problem of singularity detection in signals. Second, a new algorithm based on a fast biorthogonal spline wavelet transform (FBSWT) is proposed. According to the experimental results presented, the efficiency of the proposed algorithm is demonstrated.

Keywords: automatic inspection, spline wavelet, fast wavelet transform, singularity detection.

1. Introduction

An automatic inspection device inspects the quality of printed circuit boards using image processing technology.

One of the measurement methods, which use the three-dimensional automatic inspection device, is the slit light projection method [1]. Its measurement principle is shown in Fig.1. The laser slit light is projected to an inspection object in the vertical direction. The CCD camera captures an image of the laser projection line on the object at an angle θ. The height H of the object is calculated based on the offset d of the laser projection line from the laser base line, by using Eq.(1).

$$H = d \times \tan\theta \cdots\cdots (1)$$

For example, part of a QFP (quad flat package) on the printed circuit board is shown in Fig.2. After soldering at the position of the solder fillet as shown in Fig.2, images of the solder fillet and lead have three cases such as Figs.3(a),(b) and (c).

When the laser slit light is projected to two very close components (solder fillet and QFP) on a printed circuit board, as shown in Fig.2, images captured by a CCD camera are obtained as shown in Figs.4~6.

In order to inspect an electronic part on the printed circuit board, we must be able to detect precisely and quickly the position of the demarcation line between two very close components on printed circuit boards. Such positions are shown by the solid lines in Fig.3 and Figs.4~6. In this paper, these positions are called the characteristic positions of images.

The quality of an object is judged according to the calculated height of the object at the characteristic position.

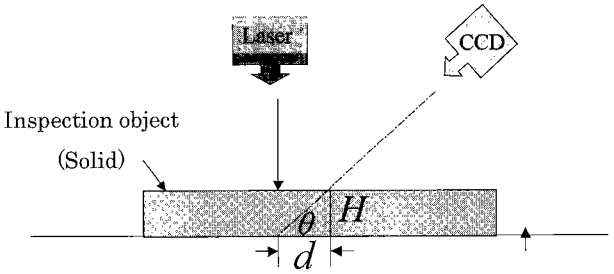

Fig. 1. Measurement principle of a three-dimensional automatic inspection device.

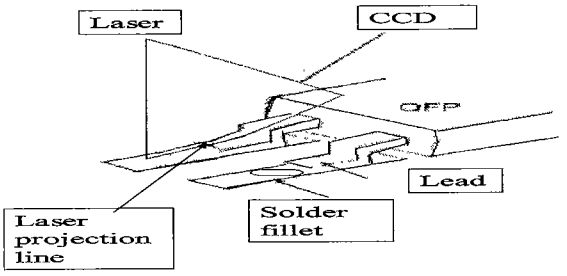

Fig. 2. Part of a QFP.

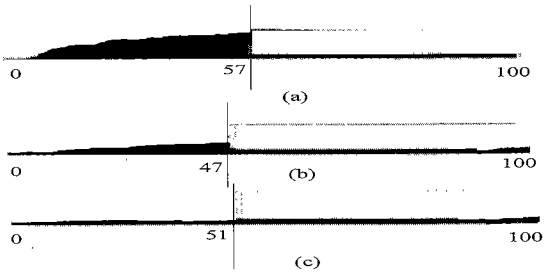

Fig. 3. Examples of images of solder fillet and lead, where (a): good solder, (b): little solder, (c): no solder.

* Graduate School of Science and Technology, Chiba University, 1-33 Yayoi-cho, Inage-ku, Chiba-shi, 263-8522, Japan. (e-mail, jiang@graduate.chiba-u.jp)

The characteristic position is calculated on the basis of the measured center coordinates and the width of electronic part by a conventional method. However, this method is low accuracy and it takes more time. In this study, we change the detection problem of the characteristic position to singularity detection in signals.

The Fourier transform [2] has been the main mathematical tool used for analyzing singularity. The Fourier transform is global and provides a description of the overall regularity of signals, but it is not well adapted for finding the location and the spatial distribution of singularity.

Recently, wavelet theory [3] has provided a unified framework for a number of techniques which were developed independently for various signal processing applications. Several singularity detection techniques [4][5] have been proposed, in which derivatives of the Gaussian function are used as wavelets. However, these techniques are not efficient in computation time because derivatives of the Gaussian function are not orthogonal, and no fast computational algorithm for dyadic decomposition exists.

In this study, to allow quick detection of the position of signal singularity, a new algorithm based on the FBSWT is proposed. On the basis of the theoretical analysis and computer simulation, the efficiency of the proposed algorithm is demonstrated.

2. Problem Transformation

In order to reduce the computational complexity, we do not apply the wavelet transform to a two-dimensional part image directly, but transform a two-dimensional part image to a one-dimensional signal in a specific format and then apply the wavelet transform. The transformation requires two steps.

The first step is to extract part images using image segmentation, where the part image is a set of pixels with high brightness, greater than a certain threshold. The second step is to calculate the center of gravity of a part image. Each center of gravity is determined by calculating the weighted mean of pixel values of the part image on each vertical sweeping pixel line.

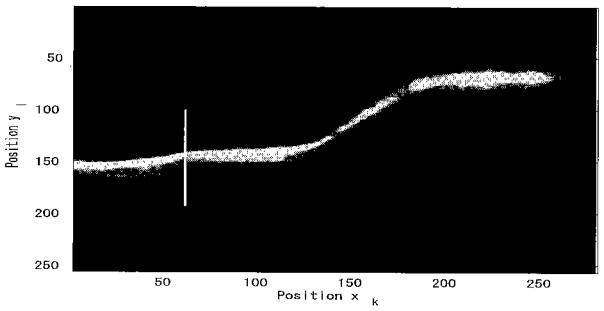

Fig. 4. Image of good solder, where the white portion of abscissa axis from 0 to 100 denotes image corresponding to Fig.3(a).

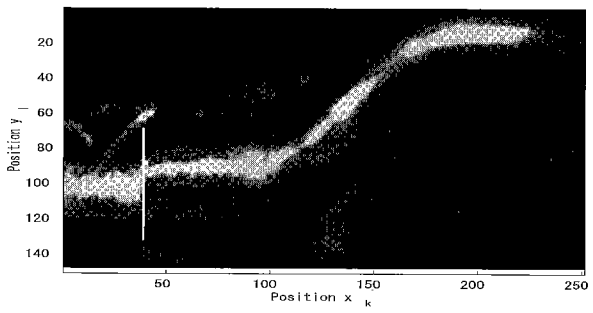

Fig. 5. Image of little solder, where the white portion of abscissa axis from 0 to 100 denotes image corresponding to Fig.3(b).

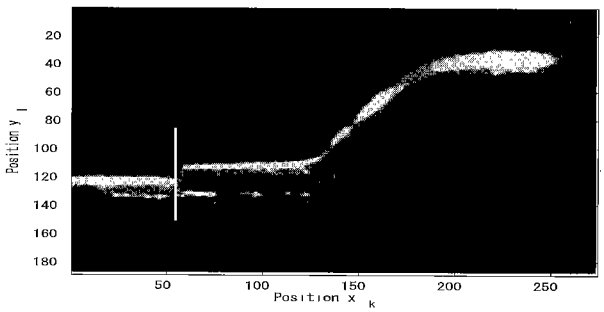

Fig. 6. Image of no solder, where the white portion of abscissa axis from 0 to 100 denotes image corresponding to Fig.3(c).

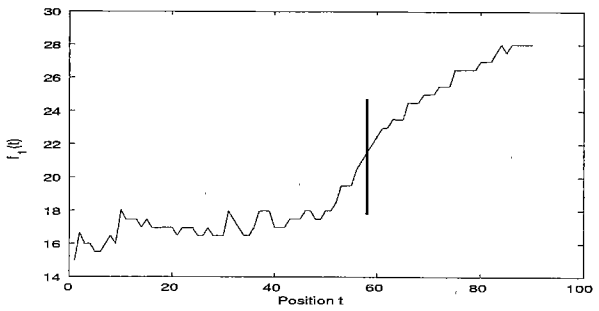

Fig. 7. Signal $f_1(t)$ corresponding to Fig.4.

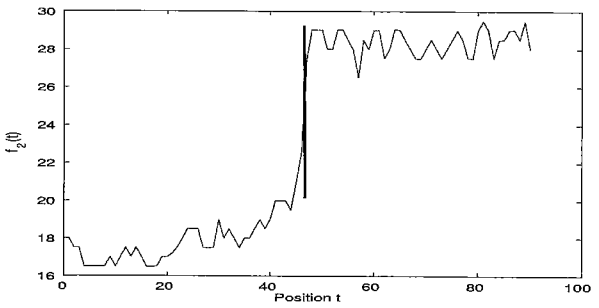

Fig. 8. Signal $f_2(t)$ corresponding to Fig.5.

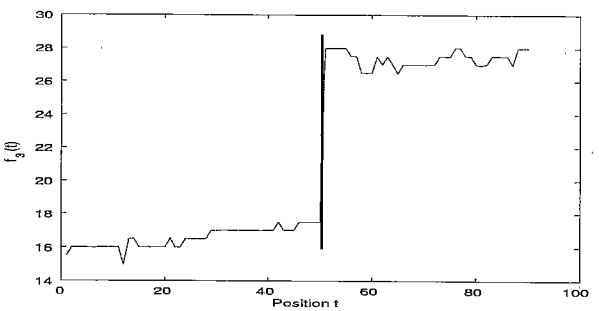

Fig. 9. Signal $f_3(t)$ corresponding to Fig.6.

A one-dimensional signal value is given by:

$$f(x_k) = \frac{1}{W_{x_k}} \sum_l w_{x_k,y_l} \times y_l, \cdots\cdots\cdots\cdots (2)$$

where (x_k, y_l) denotes the position coordinate of the part image, k and l denote the index numbers of the position coordinate of the part image in each sweeping line, w_{x_k,y_l} is the density value of the part image at (x_k, y_l), $W_{x_k} = \sum_l w_{x_k,y_l}$, and x_k denotes the position coordinate of the transformed signal, $x_k = 1, 2, 3, 4, \cdots, 90$ in this study.

To simplify, we set $t = x_k$ in the following.

By this method, we obtain signals $f_i(t)(i = 1, 2, 3)$, where $f_1(t)$ denotes the transformed signal from the image of good solder in Fig.4, $f_2(t)$ denotes the transformed signal from the image of little solder in Fig.5, and $f_3(t)$ denotes the transformed signal from the image of no solder in Fig.6. These signals are shown in Figs.7∼9, respectively.

Next, the problem for detecting the positions of the demarcation lines in Figs.4∼6 is transformed into a problem for detecting the positions of the demarcation points in Figs.7∼9, respectively.

Because these demarcation points are singularities of signals $f_i(t)(i = 1, 2, 3)$ based on their physical behavior, this is a problem of singularity detection in signals.

In this way, we can not only uniquely represent two-dimensional part images more efficiently but also achieve calculation simplicity.

3. A Fast Biorthogonal Wavelet Transform

The wavelet transform (WT) is a powerful signal processing technique, whose uniqueness lies in its ability to map the frequency content of a signal as a function of the original domain, offering the possibility of time-frequency localization. For a detailed description of the WT and of its properties, references are given to dedicated literature [6]∼[9] and only a brief description is provided here.

Biorthogonal wavelet systems can be built through two-channel biorthogonal filter banks. Fig.10 shows the block diagram of the two-channel biorthogonal filter bank. Here, $\tilde{h}$ and $\tilde{g}$ denote the low-pass and high-pass filters for decomposition, respectively, and h and g denote the low-pass and high-pass filters for reconstruction, respectively.

The decomposition is performed by applying two filters, $\tilde{h}$ and $\tilde{g}$, to the original signal: a low-pass filter $\tilde{h}$ only retaining the approximations that are the high-scale, low-frequency components of the original signal, and a high-pass filter $\tilde{g}$, collecting the details that are the low-scale, high-frequency components of the original signal. The procedure can be recursively applied by applying the same two filters to the approximation vector, until the length of the resulting vector equals 1, as shown in Fig.11.

The two-channel biorthogonal filter bank convolves an approximation A_{j-1} at level $j-1$ with a low-pass filter

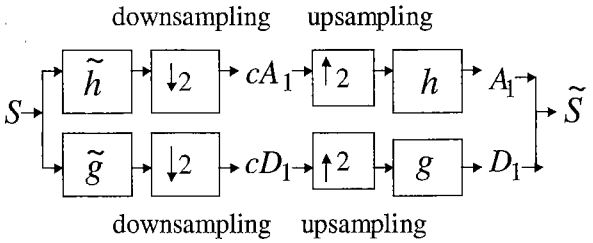

Fig. 10. Two-channel biorthogonal filter bank.

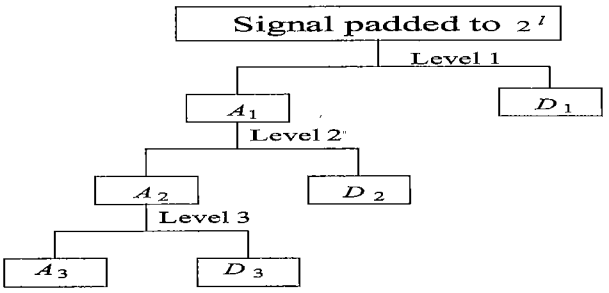

Fig. 11. Mallat's pyramid algorithm. A_i and D_i $(i = 1, 2, 3)$ denote approximations and details, respectively.

$\tilde{h}$ and a high-pass filter $\tilde{g}$ and subsamples by 2. The outputs are wavelet approximation coefficient cA_j and detail coefficient cD_j at level j, as follows:

$$cA_j(k) = A_{j-1} * \tilde{h}[2n], \cdots\cdots\cdots\cdots (3)$$

$$cD_j(k) = A_{j-1} * \tilde{g}[2n], \cdots\cdots\cdots\cdots (4)$$

where S is an input signal, and $A_0 = S$.

For each level of decomposition, j, it is possible to obtain a perfect reconstruction of the original signal by inverse WT, using the approximation at level j and all of the details from j to 1 level.

The reconstruction is performed by inserting zeros and filtering with dual filters h and g of filters $\tilde{h}$ and $\tilde{g}$ [8], as shown in Fig.10:

$$A_j[n] = \breve{cA}_j * h[n], \cdots\cdots\cdots\cdots (5)$$

$$D_j[n] = \breve{cD}_j * g[n], \cdots\cdots\cdots\cdots (6)$$

$$A_{j-1} = A_j + D_j, \cdots\cdots\cdots\cdots (7)$$

where the notation $\breve{d}[n] = \begin{cases} d[p] & n = 2p \\ 0 & n = 2p+1 \end{cases}$.

Then the reconstruction $\tilde{S}$ of the input signal S can be obtained as $\tilde{S} = A_1 + D_1$.

4. Analysis of Fast Biorthogonal Wavelet Transforms of Signals

In 1992, Mallat and Hwang [2] found the relation between the WT and signal singularities. When the scale is sufficiently small, the WT modulus maxima indicate the locations of the sharp variation points of signals and their singular degree can often be measured from their evolution across scales.

Although Mallat and Hwang's work presents satisfactory results for singularity detection in theory, the method of choosing a wavelet and scale parameters requires further study for various actual applications.

On the other hand, several computer vision researchers have proved [8] that for any finite energy signal, if the wavelet function is given by $\psi_n(t) = (-1)^n \theta^{(n)}(t)$, where $\theta(t)$ is a Gaussian function and $n = 1, 2, 3, \cdots$, the wavelet transform modulus maximum (WTMM) line belongs to connected curves that are never interrupted when the scale decreases. Therefore, the derivative of the Gaussian function is a better choice for singularity detection.

In reference (10), we have proposed an efficient algorithm in which the wavelet is the first degree derivative of the Gaussian function for detecting the characteristic position. This method has solved the low-accuracy problem, however, the derivative of the Gaussian function is not orthogonal, and no fast computational algorithm for dyadic decomposition exists, and this method also has a high computational cost problem and thus may not be suitable for real-time implementation.

Mallat and Zhong [11] proposed a spline wavelet which is similar to the derivative of the Gaussian function. We have reviewed the families of biorthogonal spline wavelets and their construction process [12]; it was found that biorthogonal spline wavelets allow the use of Mallat's fast algorithm, have space saving coding, are compactly supported, have FIR filters, and have a fixed number of vanishing moment. These properties make the biorthogonal spline wavelets a good choice for singularity detection.

Figs.12 ~15 display biorthogonal spline wavelets from the first degree to the fourth degree.

The WT coefficients indicate how closely correlated the wavelet is with this section of the signal based on wavelet theory analysis [8]. The larger the WT coefficients become, the greater the similarity becomes. More precisely, if the signal energy and the wavelet energy are equal to one, the WT coefficients may be interpreted as correlation coefficients.

In this study, our goal is to perform feature selection from signals $f_i(t)(i = 1, 2, 3)$ by using the WT. Therefore, we should choose spline wavelets such that they have better similarity with signals $f_i(t)(i = 1, 2, 3)$ in terms of their wave shapes.

On the other hand, the support size of the spline wavelets increases with their degrees, as shown in Figs.12 ~15. Therefore, a higher degree spline wavelet transform takes more time.

For the above two reasons, we choose the third degree spline wavelet to decompose $f_1(t)$ and the first degree spline wavelet to reconstruct $f_1(t)$, and the fourth order spline wavelet to decompose $f_i(t)(i = 2, 3)$ and the second degree spline wavelet to reconstruct $f_i(t)(i = 2, 3)$.

Filter coefficients of these biorthogonal spline wavelets are listed in Table 1 [12].

We assume the test scales to be 2^j with levels from $j = 1$ to $j = 5$. Then, the FBSWT is executed with signals $f_i(t)(i = 1, 2, 3)$.

We execute the FBSWT to signals $f_i(t)(i = 1, 2, 3)$ with a large number of different spline wavelets. It is found that the chosen spline wavelets are able to stress the features of the characteristic positions of signals $f_i(t)(i = 1, 2, 3)$. The results of the FBSWT of these

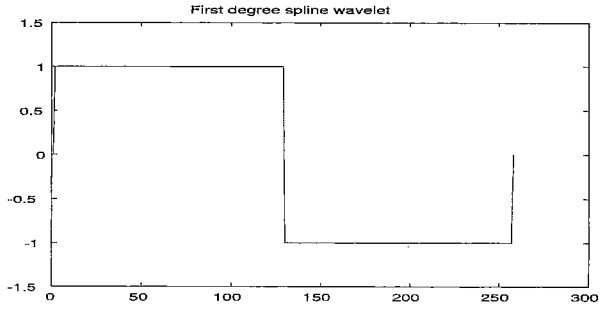

Fig. 12. First degree biorthogonal spline wavelet.

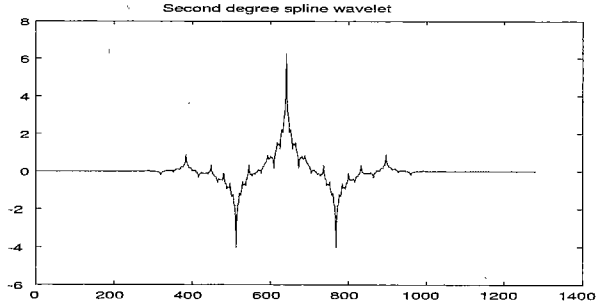

Fig. 13. Second degree biorthogonal spline wavelet.

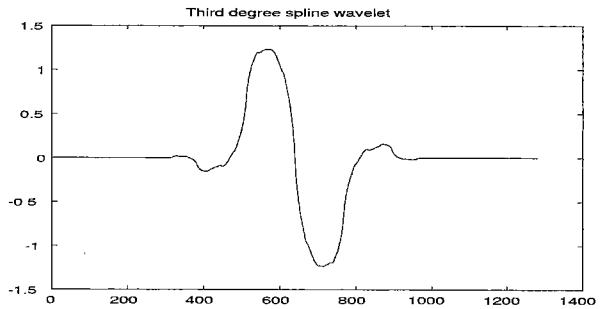

Fig. 14. Third degree biorthogonal spline wavelet.

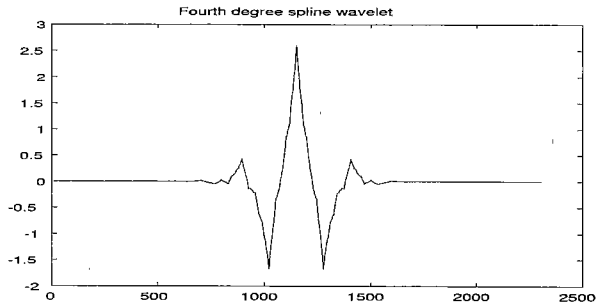

Fig. 15. Fourth degree biorthogonal spline wavelet.

Table 1. Filter coefficients of biorthogonal spline wavelets.

$h/\sqrt{2}$	$\tilde{h}/\sqrt{2}$
1/2, 1/2	−1/16, 1/16, 1/2, 1/16, −1/16
1/4, 1/2, 1/4	3/128, −3/64, −1/8, 19/64, 45/64, 19/64, −1/8, −3/64, 3/128

signals are shown in Figs.16~18, respectively.

Clearly, Figs.16~18 show the WT modulus maxima in the neighborhood of the characteristic position.

Since the scales are also linked to the time taken for the WT, we consider the problem of fine scales in the following.

The results of Figs.16~18 also show that the range of the WT modulus maxima at the characteristic position increases when the scale increases. Furthermore, the numbers of modulus maxima at large scale are much fewer than those at small scale.

Therefore, considering both the precision in automatic inspection and the speed of numerical calculation, we set the scales to be from 2^1 to 2^4 based on the observation method and search for the modulus maxima from large to small scale.

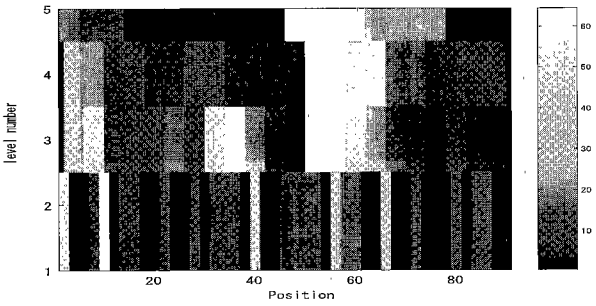

Fig. 16. Fast biorthogonal wavelet transform of signal $f_1(t)$, where decomposition wavelet is the third degree spline wavelet and reconstruction wavelet is the first degree spline wavelet.

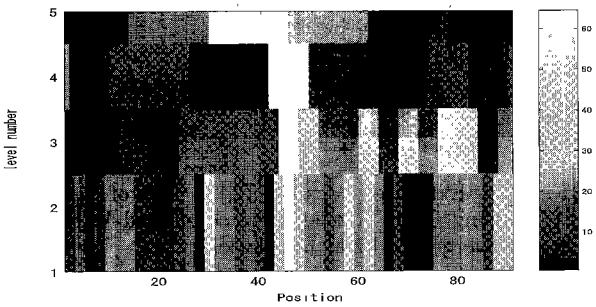

Fig. 17. Fast biorthogonal wavelet transform of signal $f_2(t)$, where decomposition wavelet is the fourth degree spline wavelet and reconstruction wavelet is the second degree spline wavelet.

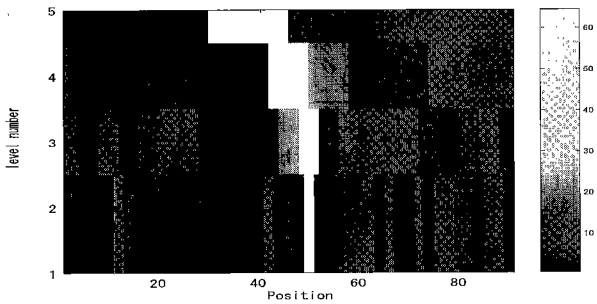

Fig. 18. Fast biorthogonal wavelet transform of signal $f_3(t)$, where decomposition wavelet is the fourth degree spline wavelet and reconstruction wavelet is the second degree spline wavelet.

5. Singularity Detection Scheme

5.1 A New Algorithm for Automatic Inspection We have presented an analysis of the characteristics with signals $f_i(t)(i = 1, 2, 3)$ in Section 4.

Based on this analysis, a simple and efficient algorithm is developed in this study.

Step 1: Signals $f_i(t)(i = 1, 2, 3)$ are decomposed using the FBSWT as shown in Eq.(3)~(6) at scales 2^j with levels $j = 1, 2, 3, 4$. These WT modulus maxima (at each level) are normalized with respect to the maximum peak at that level. Figs.19(a),(b),(c),(d)~21(a),(b),(c),(d) show the calculated results of signals $f_i(t)(i = 1, 2, 3)$ using Eq.(4) and Eq.(6) at level $j = 1, 2, 3, 4$, respectively.

Step 2: The events (possible singularities) are observed

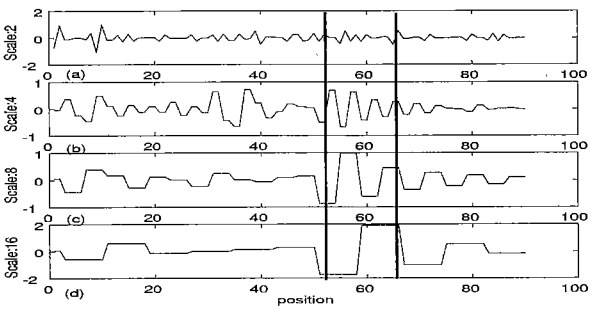

Fig. 19. Obtained details of signal $f_1(t)$, where (a): the detail at level 1, (b): the detail at level 2, (c): the detail at level 3, (d): the detail at level 4.

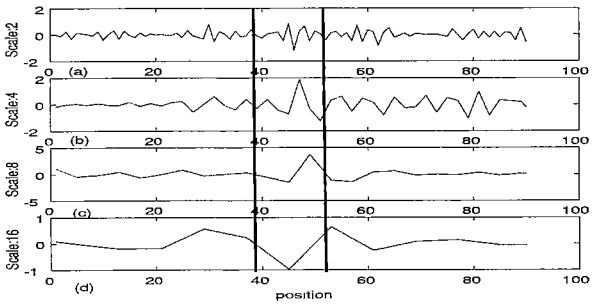

Fig. 20. Obtained details of signal $f_2(t)$, where (a): the detail at level 1, (b): the detail at level 2, (c): the detail at level 3, (d): the detail at level 4.

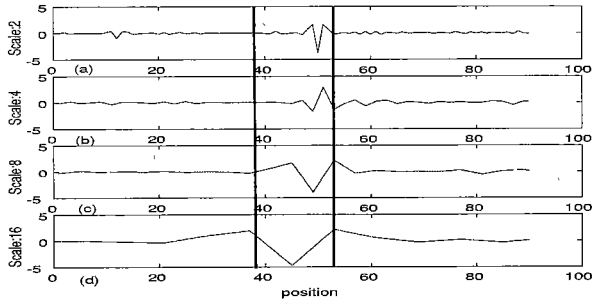

Fig. 21. Obtained details of signal $f_3(t)$, where (a): the detail at level 1, (b): the detail at level 2, (c): the detail at level 3, (d): the detail at level 4.

at the highest scale (2^4). Peaks higher than a certain threshold are recognized as valid events.

Step 3: The search range $[t_0 - 7, t_0 + 7]$ of a singular point t_0 is set up based on the valid events in Step 2.

On the basis of the calculated results in Step 3, the search ranges of signals $f_i(t)(i = 1, 2, 3)$ are set up as $[52, 66]$, $[38, 52]$ and $[38, 52]$, respectively, as shown in Figs.19~21.

Step 4: These events are successively tracked at lower scales $2^j(j = 1, 2, 3)$ to find their locations in the set search ranges in Step 3.

Step 5: The abscissas $t_m(m = 1, 2, 3, 4)$ which correspond to the WT modulus maxima at scales $2^j(j = 1, 2, 3, 4)$ in the set search ranges of these events are recorded.

Step 6: The position of each singularity is detected by using Eq.(8).

$$t_0 = \frac{1}{4}\sum_{m=1}^{4} t_m \cdots\cdots\cdots\cdots\cdots\cdots\cdots\cdots\cdots\cdots (8)$$

5.2 Computer Simulation Results In this subsection, we show the results of simulation of the signals $f_i(t)(i = 1, 2, 3)$ using the proposed algorithm. Detected results are shown in Table 2. On the basis of Table 2, at the level $j = 4$, the detected positions of singularities in signals $f_i(t)(i = 1, 2, 3)$ are at 59 pixel, 45 pixel, and 45 pixel, respectively. These are consistent with the results shown in Figs.19(d)~21(d), respectively. At the other levels $(j = 1, 2, 3)$, also, the detected positions of singularities in signals $f_i(t)(i = 1, 2, 3)$ are consistent with the results shown in Figs.19(a),(b),(c)~21(a),(b),(c), respectively.

From these detected positions of singularities in signals $f_i(t)(i = 1, 2, 3)$ at each level and using Eq.(8), we obtained that the positions of singularities in signals $f_i(t)(i = 1, 2, 3)$ are at 58 pixel, 46.75 pixel, and 48.75 pixel, respectively. The errors of these detected positions compared with the standard positions are 1 pixel, 0.25 pixels, and 2.25 pixels, respectively. The maximum detected error is 2.25 pixels.

In the development of the three-dimensional automatic inspection device, if the detected error is smaller than 5 pixels, it does not impair the quality of the device. Therefore, the detected error of the proposed algorithm is a permissible error. The efficiency of the proposed algorithm is demonstrated.

6. Comparison with the Gaussian Wavelet Based Method

In reference (10), we have proposed an efficient algorithm for detecting singularity in signals using the Gaussian continuous wavelet transform (GCWT). The local WTMM line of signals $f_i(t)(i = 1, 2, 3)$ can be extracted by using GCWT, as shown in Figs.22 ~24. We have detected the positions of singularities in $f_i(t)(i = 1, 2, 3)$ at 57 pixel, 47 pixel, and 51 pixel, respectively, by finding the abscissa where the connected WTMM line converges at a fine scale.

A comparison of the proposed algorithm and the Gaussian wavelet based method [10] (GCWT method) is performed. Table 3 shows the results obtained by the proposed algorithm and the GCWT method. It is found that the performance of the proposed algorithm is similar to the GCWT method in terms of precision.

Quantitatively, we have compared the time taken for

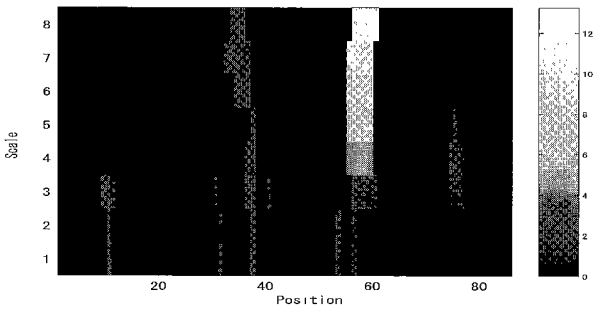

Fig. 22. Extracted local WTMM line of signals $f_1(t)$ using GCWT, where the connected WTMM line converged to 57 at fine scale.

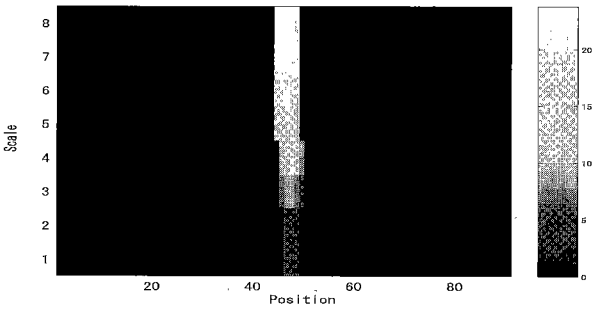

Fig. 23. Extracted local WTMM line of signals $f_2(t)$ using GCWT, where the connected WTMM line converged to 47 at fine scale.

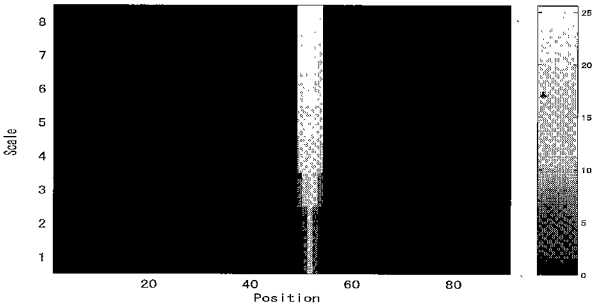

Fig. 24. Extracted local WTMM line of signals $f_3(t)$ using GCWT, where the connected WTMM line converged to 51 at fine scale.

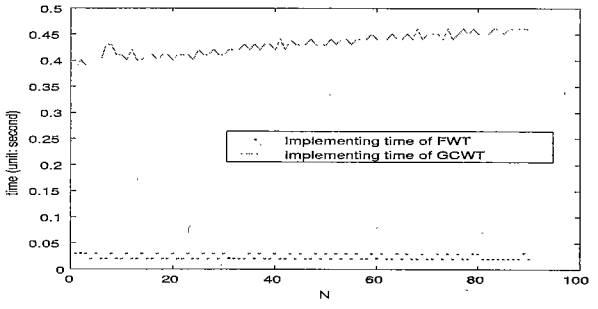

Fig. 25. Comparison of the implementing time of the two methods, using processor x86 Family 6 Model 8 Stepping 3 GenuineIntel 702 MHz.

Table 2. Detected results of signals $f_i(t)(i = 1, 2, 3)$.

Signal	Levels	Possible positions				Detected position	Standard position	Error
$f_1(t)$	1 to 4	59	56	58	59	58	57	1
$f_2(t)$	1 to 4	46	47	49	45	46.75	47	0.25
$f_3(t)$	1 to 4	50	51	49	45	48.75	51	2.25

Table 3. Comparison of the detected results of two methods for signals $f_i(t)(i = 1, 2, 3)$.

Signal	Proposed method	GCWT method	Standard position	New error	Old error
$f_1(t)$	58	57	57	1	0
$f_2(t)$	46.75	47	47	0.25	0
$f_3(t)$	48.75	51	51	2.25	0

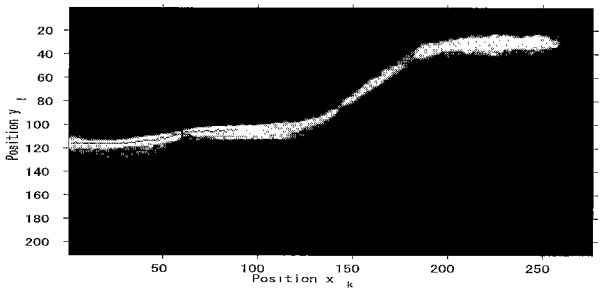

Fig. 26. Detected position in Fig.4, where the solid curve denotes the signal transformed by using Eq.(2) and the plus sign denotes the characteristic position detected by using the proposed algorithm.

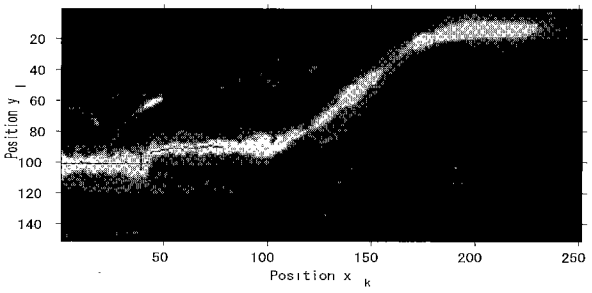

Fig. 27. Detected position in Fig.5, where the solid curve denotes the signal transformed by using Eq.(2) and the plus sign denotes the characteristic position detected by using the proposed algorithm.

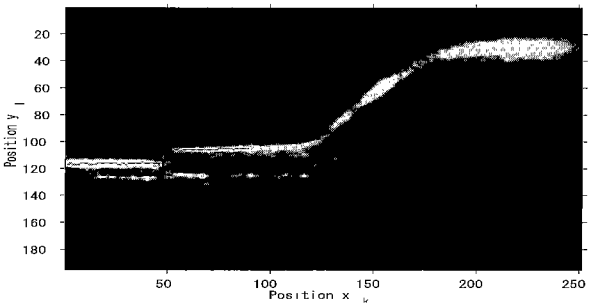

Fig. 28. Detected position in Fig.6, where the solid curve denotes the signal transformed by using Eq.(2) and the plus sign denotes the characteristic position detected by using the proposed algorithm.

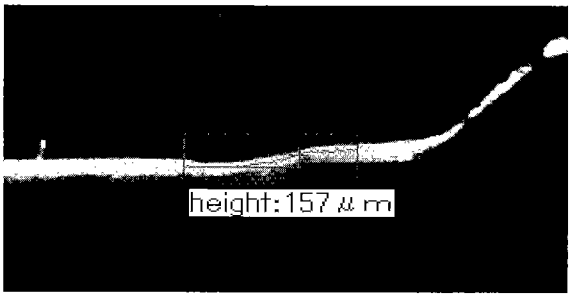

Fig. 29. Good electronic part (inspection result of the electronic part in Fig.4).

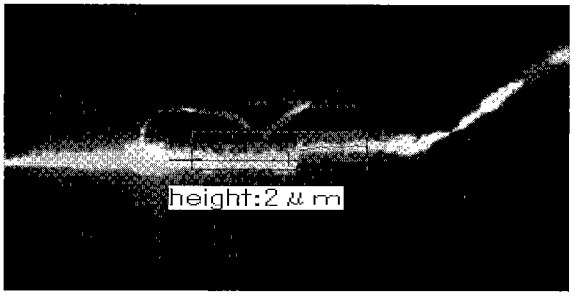

Fig. 30. No good electronic part (inspection result of the electronic part in Fig.5).

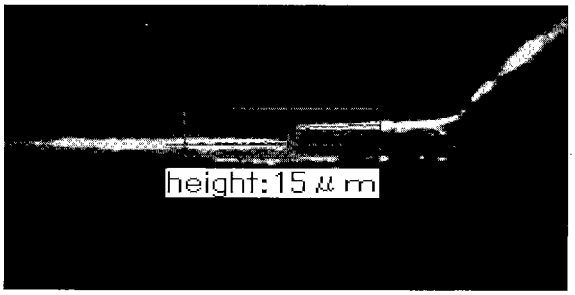

Fig. 31. No good electronic part (inspection result of the electronic part in Fig.6).

the GCWT of signal $f_1(t)$ used in reference (10) and the FBSWT of signal $f_1(t)$ used in this study, where the processor used is an x86 Family 6 Model 8 Stepping 3 GenuineIntel 702 MHz. The obtained results are displayed in Fig.25, where the dotted line denotes the implementing time of the GCWT method, and the point line denotes the implementing time of the proposed method. Clearly, Fig.25 shows that the implementing time of the GCWT method gradually increases to 0.471 seconds with increasing t, and the implementing time of the proposed method tends to retain 0.02 seconds with increasing t. Therefore, the FBSWT used in this study is significantly more efficient.

In the proposed algorithm, we have used the FBSWT for decomposing signals and the scales are chosen from 2^1 to 2^4. Furthermore, the modulus maxima are

Table 4. Inspection results for different electronic parts.

Part images	Calculated height	Interval of inspection criterion	Inspection results
Part 1(Good solder)	157 μm	[100, 220]	G
Part 2(Little solder)	2 μm	[100, 220]	NG
Part 3(No solder)	15 μm	[100, 220]	NG
Part 4(No solder)	18 μm	[100, 220]	NG
Part 5(Good solder)	157 μm	[100, 220]	G
Part 6(Good solder)	153 μm	[100, 220]	G
Part 7(Good solder)	165 μm	[100, 220]	G
Part 8(Little solder)	13 μm	[100, 220]	NG
Part 9(Little solder)	22 μm	[100, 220]	NG
Part 10(No solder)	3 μm	[100, 220]	NG

searched from large to small scale in the set search range of possible singularities. Therefore, the proposed technique has the advantage in real-time processing compared with the other techniques [4],[5],[10].

7. Application to Three-Dimensional Automatic Inspection Device

We have applied the proposed algorithm to more than 20 actual images obtained from the three-dimensional automatic inspection device. It is demonstrated that the proposed algorithm can succcessfully detect the position of the demarcation line between two very close components on a printed circuit board. Also, we have conducted the direct simulation of actual images in Figs.4~6. Figs.26~28 show the obtained simulation results. In these figures, the solid curves denote the signals transformed by using Eq.(2) and the plus signs denote the characteristic positions detected by using the proposed algorithm. On the basis of Figs.26~28, we found that the detected characteristic positions are consistent with the positions shown in Figs.4~6.

We have also applied the proposed algorithm to the development of a software system for the three-dimensional automatic inspection device. The height of the object at the detected characteristic position is calculated by using Eq.(1). The quality of the object is judged according to the calculated height. In fact, the height of a electronic part in a printed circuit board has a special demand. The special demand is set up as the interval of inspection criterion in this study. If the calculated height of the electronic part is within the interval of the inspection criterion, the quality of this electronic part is judged to be good (G), otherwise the quality of this electronic part is judged to be no good (NG).

Regarding the part images used in this study, the interval of the inspection criterion is set up as $[100, 220]$. Table 4 shows inspection results for different electronic parts. Parts 1~3 in Table 4 denote electronic parts corresponding to images in Figs.4~6, respectively. Figs.29~31 show their inspection results.

On the basis of Table 4, the calculated heights of electronic parts corresponding to images of good solder are found to be in the interval of the inspection criterion $[100, 220]$, and the quality of these objects therefore is judged to be good. The calculated heights of electronic parts corresponding to images of little solder and no solder are outside the interval of the inspection criterion $[100, 220]$, and the quality of these objects is judged to be no good. Therefore, the quality of the object is successfully judged.

8. Conclusion

In this paper, a new algorithm that is based on the FBSWT has been proposed for solving an automatic inspection problem. Some detection results have been shown. The experimental results have shown that the proposed algorithm can successfully specify the location of these singularities. Also, the proposed algorithm has been applied to the development of the software system of the three-dimensional automatic inspection device. The quality of the object was successfully judged according to the calculated height of the object at the detected positions. We observed that the proposed method not only gave the results which were competitive with those of the other available techniques but also had the advantage of real-time performance.

(Manuscript received Oct. 3, 2002,
revised March 17, 2003)

References

(1) T. Yoshizawa: Three-Dimensional Light Measurement, New Technical Communications Pub., (1998)
(2) T. Yahagi: Digital Signal Processing and Basic Theory, Corona Pub., Tokyo Japan (1996)
(3) S. Mallat and W.L. Hwang: "Singularity detection and processing with wavelets", *IEEE Trans. Inform. Theory*, Vol.38, No.2, pp.617–643 (1992)
(4) J.C. Hong, Y.Y. Kim, H.C. Lee, and Y.W. Lee: "Damage detection using the Lipschitz exponent estimated by the wavelet transform: applications to vibration modes of a beam", *International Journal of Solids and Structures*, Vol.39, pp.1803–1816 (2002)
(5) M.I. Khalil and M.M. Bayoumi: "Invariant 2D object recognition using the wavelet modulus maxima", *Pattern recognition Letters*, Vol.21, pp.863–872 (2000)
(6) G. Strang and T. Nguyen, Editors: Wavelet and Filterbanks, Wellesey Cambridge Press, Wellesey, MA (1996)
(7) I. Daubechies: Ten Lectures on Wavelets, SIAM Press, Philadelphia, USA (1992)
(8) S. Mallat: A Wavelet Tour of Signal Processing, Academic Press, San Diego (1998)
(9) S. Mallat: "A theory for multiresolution signal decomposition: the wavelet representation", *IEEE Pattern Anal. and Machine Intell.*, Vol.11, No.7, pp.674–693 (1989)
(10) H. Jiang, T. Yahagi, and J. Lu: "An efficient algorithm for detecting singularity in signals using wavelet transform", Proceedings of the 2002 IEICE general conference, A-4-27 (2002)
(11) S. Mallat and S. Zhong: "Characterization of signals from multiscale edges", *IEEE Trans. Pattern Anal. Machine Intelligence*, Vol.14, No.7, pp.710–732 (1992)
(12) H. Jiang, J. Lu, and T. Yahagi: "B-spline approximation and

fast wavelet transforms for singularity detection", *IEEE International Symposium on Intelligent Signal Processing and Commun. Syst., Kaohsiung*, Taiwan, pp.468–472 (2002)

Appendix

Here, we present some comparisons with other means of time-frequency analysis such as Fourier analysis and the short-time Fourier transform (STFT).

Fourier analysis has been the main mathematical tool used for analyzing singularities, but Fourier analysis has a serious drawback. In transforming to the frequency domain, time or position information is lost. When viewing a Fourier transform of a signal, it is impossible to tell when or where a particular event took place. app.Fig.1 shows a plot of the Fourier coefficients of the signal $f_1(t)$. From this figure, we cannot obtain any information on the singularity positions.

The STFT provides some information about both when (where) and at what frequencies a signal event occurs. However, we can only obtain this information with limited precision, and that precision is determined by the size of the window. app.Fig.2 shows the STFT of the signal $f_1(t)$, where the window function is a hamming window of length 20 and sampling frequency is 2000 H_z. Again, we cannot obtain any information on the singularity positions from app.Fig.2.

Wavelet analysis represents the next logical steps, a windowing technique with variable-sized regions. Wavelet analysis allows the use of long time intervals in cases where we want more precise low-frequency information, and in shorter regions where we want high-frequency information. Based on such wavelet properties and the obtained results in this study, it has been shown that one major advantage afforded by wavelets is the ability to perform local analysis namely to analysis a localized area of a larger signal.

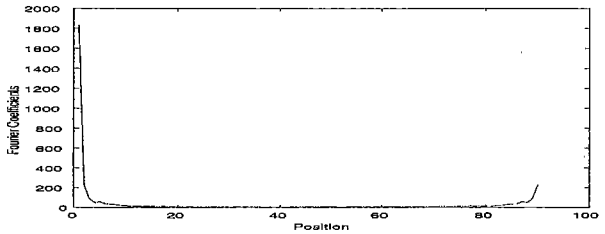

app. Fig. 1. Fourier coefficients of signal $f_1(t)$.

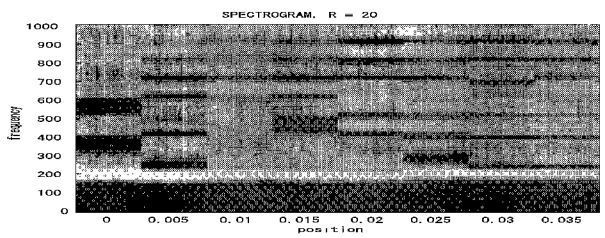

app. Fig. 2. STFT of signal $f_1(t)$, where window function is hamming window of length 20.

Huiqin Jiang (Non-member) received the M.S. degrees in Applied Mathematics from Zhengzhou University, Zhengzhou, P. R. China., in 1988. In 1988, she joined Zhengzhou University of Technology, Zhengzhou, P. R. China., as a Lecturer in the Department of Mathmatics and Mechanics. From Sep.1988 to Sep.1997, she was Assistant Professor. From Sep.1997 to Mar.1999, she was Associate Professor. From Apr.1999 to Mar.2001., she joined Tokyo Research Institute of Tani Electronic Company, Tokyo, Japan, as a Senior-level Software Engineer to develop the software system of the automatic image inspector. In April 2001, she joined the Graduate School of Science and Technology of Chiba University, Japan, as a Ph. D. student. Her current research interests include the theory and applications of digital signal processing using wavelet transforms and medical image processing. She is a member of IEICE (Japan), Research Institute of Signal Processing, Japan.

Jianming Lu (Member) received the M.S., and Ph.D. degrees from Chiba University, Japan, in 1990 and 1993, respectively. In 1993, he joined Chiba University, Chiba, Japan, as an Associate in the Department of Information and Computer Sciences. Since 1994 he has been with the Graduate School of Science and Technology, Chiba University, and in 1998 he was promoted to Associate Professor in the Graduate School of Science and Technology, Chiba University. His current research interests are in the theory and applications of digital signal processing and control theory. Dr. Lu is a member of IEICE (Japan), SICE (Japan), IEEJ (Japan) and JSME (Japan), Research Institute of Signal Processing, Japan, etc.

Takashi Yahagi (Non-member) received the B. S., M. S., and Ph.D. degrees in electronics from the Tokyo Institute of Technology, Tokyo, Japan, in 1966, 1968, 1971, respectively. In 1971, he joined Chiba University, Chiba, Japan, as a Lecturer in the Department of Electronics. From 1974 to 1984 he was an Associate Professor, and in 1984 he was promoted to Professor in the Department of Electrical Engineering. From 1989 to 1998, he was with the Department of Information and Computer Sciences. Since 1998 he has been with the Department of Information Science of the Graduate School of Science and Technology, Chiba University. His current research interests are in the theory and applications of digital signal processing and other related areas. He is the author of "Theory of Digital Signal Processing", Vols. 1-3 (1985, 1985, 1986), and "Digital Signal Processing and Basic Theory" (1996), "Digital Filters and Signal Processing" (2001) and the co-author of "Digital Signal Processing of Speech and Images" (1996), "VLSI and Digital Signal Processing" (1997), "Multimedia and Digital Signal Processing" (1997), "Neural Network and Fuzzy Signal Processing" (1998), "Communications and Digital Signal Processing" (1999), "Fast Algorithms and Parallel Signal Processing" (2000) (Corona Pub. Co., Ltd., Tokyo, Japan). He is Editor of the "Library of Digital Signal Processing" (Corona Pub. Co., Ltd., Tokyo, Japan). Since 1997, he has been President of the Research Institute of Signal Processing, Japan, and also Editor-in-Chief of the Journal of Signal Processing. Prof. Yahagi is a member of IEEE (USA), IEICE (Japan), Research Institute of Signal Processing, Japan, etc.